

Synchrotron Characterization of Nano-grained UO_2 Grain Growth

Nuclear Engineering Division

About Argonne National Laboratory

Argonne is a U.S. Department of Energy laboratory managed by UChicago Argonne, LLC under contract DE-AC02-06CH11357. The Laboratory's main facility is outside Chicago, at 9700 South Cass Avenue, Argonne, Illinois 60439. For information about Argonne and its pioneering science and technology programs, see www.anl.gov.

DOCUMENT AVAILABILITY

Online Access: U.S. Department of Energy (DOE) reports produced after 1991 and a growing number of pre-1991 documents are available free via DOE's SciTech Connect (<http://www.osti.gov/scitech/>)

Reports not in digital format may be purchased by the public from the National Technical Information Service (NTIS):

U.S. Department of Commerce
National Technical Information Service
5301 Shawnee Rd
Alexandria, VA 22312
www.ntis.gov
Phone: (800) 553-NTIS (6847) or (703) 605-6000
Fax: (703) 605-6900
Email: orders@ntis.gov

Reports not in digital format are available to DOE and DOE contractors from the Office of Scientific and Technical Information (OSTI):

U.S. Department of Energy
Office of Scientific and Technical Information
P.O. Box 62
Oak Ridge, TN 37831-0062
www.osti.gov
Phone: (865) 576-8401
Fax: (865) 576-5728
Email: reports@osti.gov

Disclaimer

This report was prepared as an account of work sponsored by an agency of the United States Government. Neither the United States Government nor any agency thereof, nor UChicago Argonne, LLC, nor any of their employees or officers, makes any warranty, express or implied, or assumes any legal liability or responsibility for the accuracy, completeness, or usefulness of any information, apparatus, product, or process disclosed, or represents that its use would not infringe privately owned rights. Reference herein to any specific commercial product, process, or service by trade name, trademark, manufacturer, or otherwise, does not necessarily constitute or imply its endorsement, recommendation, or favoring by the United States Government or any agency thereof. The views and opinions of document authors expressed herein do not necessarily state or reflect those of the United States Government or any agency thereof, Argonne National Laboratory, or UChicago Argonne, LLC.

Synchrotron Characterization of Nano-grained UO₂ Grain Growth

prepared by
Kun Mo, Yinbin Miao, Di Yun, and Laura M. Jamison
Nuclear Engineering Division, Argonne National Laboratory

Jie Lian and Tiankai Yao
Rensselaer Polytechnic Institute

prepared for
U.S. Department of Energy
Nuclear Energy Advanced Modeling & Simulation Program

September 30, 2015

ABSTRACT

This activity is supported by the US Nuclear Energy Advanced Modeling and Simulation (NEAMS) Fuels Product Line (FPL) and aims at providing experimental data for the validation of the mesoscale simulation code MARMOT. MARMOT is a mesoscale multiphysics code that predicts the coevolution of microstructure and properties within reactor fuel during its lifetime in the reactor. It is an important component of the Moose-Bison-Marmot (MBM) code suite that has been developed by Idaho National Laboratory (INL) to enable next generation fuel performance modeling capability as part of the NEAMS Program FPL. In order to ensure the accuracy of the microstructure based materials models being developed within the MARMOT code, extensive validation efforts must be carried out. In this report, we summarize our preliminary synchrotron radiation experiments at APS to determine the grain size of nano-grain UO_2 . The methodology and experimental setup developed in this experiment can directly apply to the proposed *in-situ* grain growth measurements. The investigation of the grain growth kinetics was conducted based on isothermal annealing and grain growth characterization as functions of duration and temperature. The kinetic parameters such as activation energy for grain growth for UO_2 with different stoichiometry are obtained and compared with molecular dynamics (MD) simulations.

CONTENTS

ABSTRACT	Error! Bookmark not defined.
1. Introduction	Error! Bookmark not defined.
1.1 Brief Introduction to the MARMOT Simulation Code.....	Error! Bookmark not defined.
1.2 The Objectives	Error! Bookmark not defined.
1.3 The Structure and Content of This Report	Error! Bookmark not defined.
2. Synchrotron Radiation Experiment.....	10
2.1 Materials and Experimental Setup	Error! Bookmark not defined.
2.1.1 Description of the Samples	Error! Bookmark not defined.
2.1.2 Experimental Setup and Sample Containment... ..	Error! Bookmark not defined.
2.2 Art of Synchrotron Scattering Data Analysis	Error! Bookmark not defined.
2.3 Results and Discussion.....	15
2.3.1 Lattice Parameter Measurement.....	15
2.3.2 The Williamson-Hall Analysis.....	16
3. Isothermal Annealing and Grain Growth Kinetics.....	21
3.1 Isothermal Annealing and Grain Growth Characterization	21
3.2 Grain Growth Kinetics	22
3.3 Grain Coarsening Kinetics	25
4. Future Work	28
5. Summary	29
6. Acknowledgements	30
7. References	31

FIGURES

Figure 1: the conventional XRD results of the samples (first three curves)**Error! Bookmark not defined.**

Figure 2: SEM image of Sample A	11
Figure 3: SEM image of Sample B	11
Figure 4: SEM image of Sample C	12
Figure 5: loaded nano-grained UO ₂ samples on Ni-based stands: (a) Sample A; (b) Sample B; (c) Sample C.	13
Figure 6: lineouts of WAXS scattering results.....	16
Figure 7: the conventional W-H analysis of Sample A.....	17
Figure 8: the modified W-H analysis of Sample B	17
Figure 9: the conventional W-H analysis of Sample B.....	18
Figure 10: the modified W-H analysis of Sample B	18
Figure 11: the conventional W-H analysis of Sample C.....	19
Figure 12: the modified W-H analysis of Sample C	19
Figure 13: XRD (111) peak position and width for 7-1-UO _{2.03} after various holding time at 700 °C (a), microstructure of 7-1-UO _{2.03} after 2 hrs (b) and 4 hrs (c) holding at 700 °C (Yao and Lian, unpublished data).	21
Figure 14: microstructure of 7-5-UO _{2.03} after 0 hr (a), 0.5 hr (b), 1 hr (c), 2 hrs (d), 4 hrs (e), and 8 hrs (f) holding at 700 °C (scale bar is 200 nm except for 100 nm in (a) and 300 nm in (b)) (Yao and Lian, unpublished data).	22
Figure 15: microstructure of 6-20-UO _{2.11} after 0 hr (a), 0.5 hr (b), 1 hr (c), 2 hrs (d), 4 hrs (e), and 8 hrs (f) holding at 700 °C (scale bars are 200 nm except for 300 nm in (d) and 100 nm in (e)) (Yao and Lian, unpublished data).	23
Figure 16: grain growth data curve fitting with fitted growth component highlighted for 7-5-UO _{2.03} (a), 7-20-UO _{2.03} (b), 6-20-UO _{2.11} (c), and 7-20-UO _{2.11} (d) (Yao and Lian, unpublished data).....	24
Figure 17: grain growth time component fitting for 7-5-UO _{2.03} (a), 7-20-UO _{2.03} (b), 6-20-UO _{2.11} (c), and 7-20-UO _{2.11} (d) (Yao and Lian, unpublished data).....	25
Figure 18: grain growth activation energy fitting for 7-5-UO _{2.03} (a), 7-20-UO _{2.03} (b), 6-20-UO _{2.11} (c), and 7-20-UO _{2.11} (d) (Yao and Lian, unpublished data).....	27

TABLES

Table 1: description of samples.....	10
Table 2: the parameters used in the calculation of contrast factors.	15
Table 3: lattice constants and stoichiometry of the samples	15
Table 4: fitting results of the conventional and modified W-H analyses.....	20

1. Introduction

1.1 Brief Introduction to the MARMOT Simulation Code

MARMOT is a mesoscale multiphysics code that predicts the coevolution of microstructure and properties within reactor fuel during its lifetime in the reactor. It is an important component of the Moose-Bison-Marmot (MBM) code suite that has been developed by Idaho National Laboratory (INL) to enable next generation fuel performance modeling capability as part of the NEAMS Program Fuels Product Line (FPL). The BISON code is a main component of the MBM code suite to provide nuclear fuel performance modeling capabilities. Many of the materials models within the BISON fuel performance code are legacy materials models that are primarily empirical fits to experimental data. Although these materials models are well established and have been used for years, they cannot provide the predictive capability required in the next generation fuel performance code. Empirical models can hardly be extrapolated outside the bounds of experimental conditions, and therefore are not applicable to new reactor concepts or ultra-high burnup scenarios of existing reactor designs. In addition, these empirical models are usually correlated to burnup of the fuels. However, burnup is not a unique measure of fuel irradiation history, as fuels can reach the same burnup via different routes and therefore have very different microstructures and properties. Thus, models that are sensitive to microstructures of fuel materials are more ideal to be used in the next generation fuel performance code. To this end, the MARMOT code emphasizes the importance of modeling the fuel material behavior and properties with microstructure-based models.

1.2 The Objectives

In order to ensure the accuracy of the microstructure-based materials models being developed within the MARMOT code, extensive validation efforts must be carried out. This year, we are focusing on the validation of grain growth models in the MARMOT code.

The proposed experiment is of both scientific and engineering significance. Nanocrystalline materials have been studied for decades for a wide range of applications, e.g., catalysis and hydrogen storage. Nanomaterials have been proposed for use in nuclear applications, but the focus of these studies has been primarily on metallic structural materials. The unique microstructure in nanomaterials, i.e., the large amount of grain boundary systems, has attracted the nuclear materials research community. The numerous grain boundaries within nanocrystalline materials have the potential to hose radiation-induced defects, and thus improve materials' radiation resistance. Improved radiation resistance is desired in the structural materials for many advanced reactors, e.g., sodium fast reactors and the traveling wave reactor. Rather than the structural applications of nanocrystalline materials, our focus in this project is on nanocrystalline (nano-grained or nano-sized) UO_2 . Nanocrystalline UO_2 already exists in fuel pellets in the LWR after high-burnup. After prolonged irradiation, the originally large-grained (10–20 μm) nuclear fuels in the outer part of the UO_2 nuclear fuel pellet suffer grain subdivision (low-angle subgrain formation) and/or recrystallization (high angle sub-grain formation) changes resulting in a new structure of nm-sized grains. This new structure is called the High Burn-up Structure (HBS). Recently, many research activities focused on the development of nano-crystalline (nc)-oxide fuels for commercial power reactors (LWR's) have emerged. These activities are aimed at promoting the HBS transformation and its assigned advantageous features as soon as possible from the onset of the irradiation. Currently, nano-grained UO_2 can be successfully fabricated by a plasma sintering process in many places around the world. However, the stability of the nano-grained fuel microstructure in the nuclear reactor environment is a primary concern for many researchers. The suspected instability stems from two main sources: thermally induced grain growth and irradiation induced grain growth. Therefore, understanding the grain growth kinetics of these nano-grained UO_2 fuel materials under both isothermal annealing conditions and athermal irradiation environments is critical. Our proposed research work specifically aims to understand the grain growth kinetics of the nano-grained UO_2 microstructure. The results of this experiment will help provide new information about the thermal

stability of the nano-grained UO_2 fuel as well as give important validation data to the MARMOT UO_2 grain growth models.

1.3 The Structure and Content of This Report

In this report, we summarize our accomplishments in grain growth study of nano-grained UO_2 for FY15. We conducted a preliminary synchrotron radiation experiment at APS to determine the grain size of nano-grained UO_2 . The methodology and experimental setup developed in this experiment applies directly to the proposed *in-situ* grain growth measurements for FY16. In addition, the investigation of grain growth kinetics was initiated based on isothermal annealing and grain growth characterization as functions of duration and temperature. The kinetic parameters, such as activation energy for grain growth in UO_2 , are obtained for different stoichiometry and compared with molecular dynamics (MD) simulations.

The first chapter of this report introduces the background for this work and summarizes our major achievements.

Chapter 2 summarizes a synchrotron radiation experiment on nano-grained UO_2 samples. The goal of this experiment is to develop a methodology for using synchrotron X-ray diffraction to measure the grain size of nano-grained UO_2 . The experimental setup, data interpretation methods, and procedures are given in detail and will apply to the *in-situ* grain growth measurement of nano-grained UO_2 during isothermal heating.

Chapter 3 summarizes our efforts in studying grain growth kinetics of nano-grained UO_2 . A systematic grain growth study of nano-sized $\text{UO}_{2.03}$ and $\text{UO}_{2.11}$ was performed with isothermal heating and SEM characterizations. This study shows significant differences in grain coarsening kinetics between nano- and large- crystalline UO_2 . Stoichiometry and porosity of the sintered UO_2 fuels were also found to significantly impact the grain coarsening process.

Chapter 4 outlines the planned experimental work for FY16. We have completed a methodology study using synchrotron X-rays to analyze grain growth in nano-grained UO_2 . The only remaining issue for the *in-situ* experiment is ensuring compliance with the stringent safety regulations for heating radioactive materials at APS. The old sample holder design for the UO_2 samples was required to include one additional layer of containment. The new design has been completed and is now under review by the safety committee at APS. The proposed *in-situ* grain growth experiment has been scheduled in the 2015-3 APS beam cycle. In addition to the grain growth experiments, we plan to perform nano-indentation/micro-hardness measurement of UO_2 materials with various grain sizes. This work aims to provide validation data for the MARMOT and BISON Fracture Model.

Finally, Chapter 5 provides a summary of the work conducted in this fiscal year.

2. Synchrotron Radiation Experiment

To provide *in-situ* grain growth data to support the grain growth model, and the potential high-burnup-structure models (formation and stability) in MARMOT, synchrotron radiation experiments were planned with isothermal annealing on nano-grained UO_2 samples. Due to the stringent safety regulation, the heating for UO_2 samples requires two-layers of containment for APS experiments. A recent containment design is still under review by the APS radiation safety committee. In FY15, we focused on the methodology development for grain size measurement of the nano-grained UO_2 samples. A preliminary synchrotron experiment was conducted at sector 1-ID at APS. The synchrotron experimental details, procedure for data analysis, and the results and discussion of the preliminary study of the nano-grained UO_2 were reported.

2.1 Materials and Experimental Setup

2.1.1 Description of the Samples

Three nano-grained UO_2 samples that were sintered under different conditions were investigated by synchrotron X-ray scattering in this study, as listed in Table 1. The samples were examined using conventional X-ray diffraction (XRD) just after sintering, as shown in Figure 1. All the three samples were found to contain a single fluorite phase.

Table 1: description of samples

Symbol	A	B	C
Sinter Temperature/ $^{\circ}\text{C}$	600	600	600
Duration Time/mins	20	20	1
Pressure/MPa	500	750	750

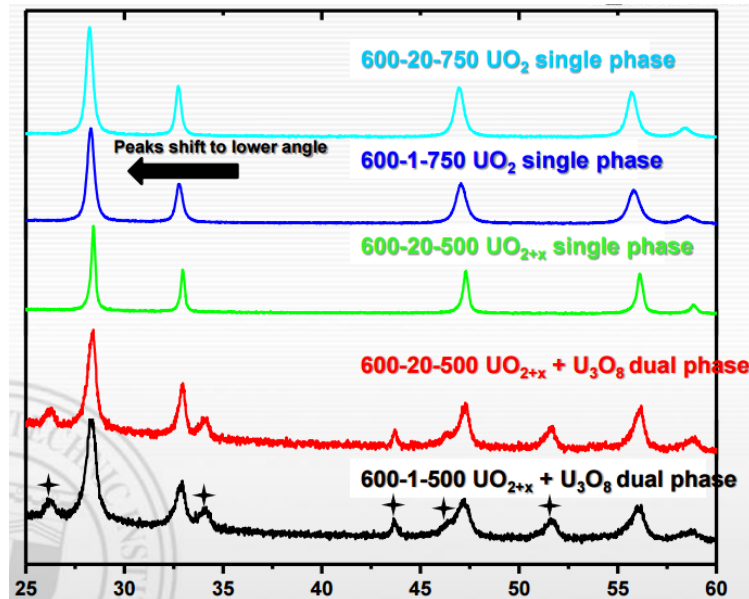


Figure 1: the conventional XRD results of the samples (first three curves)

SEM has also been utilized to provide the morphology of the grains within the samples. Figures 2 through 4 illustrate the basic morphology of the three sintered samples by means of SEM imaging. The grain size of Sample A was measured as 99 ± 21 nm. The grain sizes of the other two samples are also around 100 nm. However, grain size measurement based on SEM image was limited to the cross sections of hundreds of grains on the surface. Therefore, in order to look comprehensively at dynamic grain growth behavior, a more efficient and reliable experimental approach is needed to provide more accurate measurement of average grain size within a larger volume free from surface effects. Synchrotron X-ray scattering, due to its unique high energy and high intensity nature, is an ideal tool for accomplishing this task.

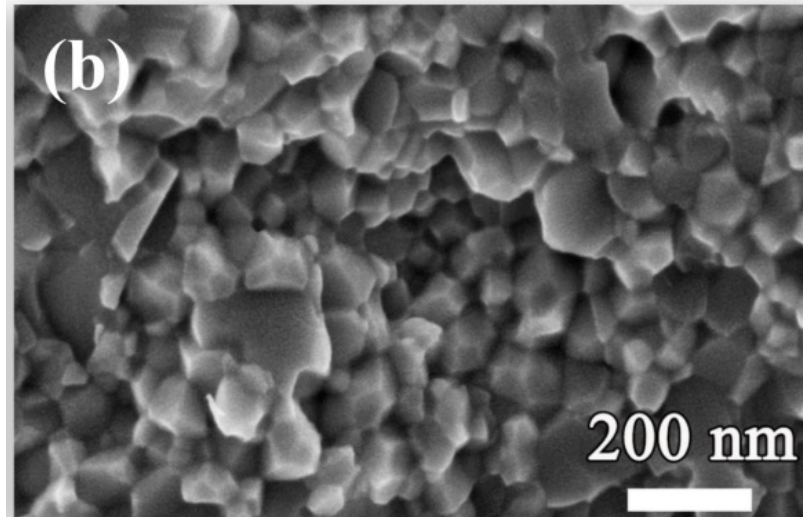


Figure 2: SEM image of Sample A

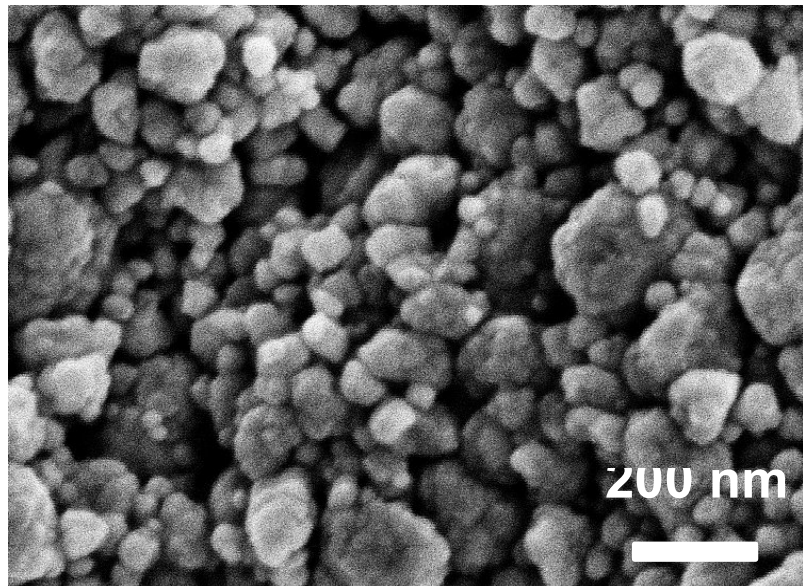


Figure 3: SEM image of Sample B

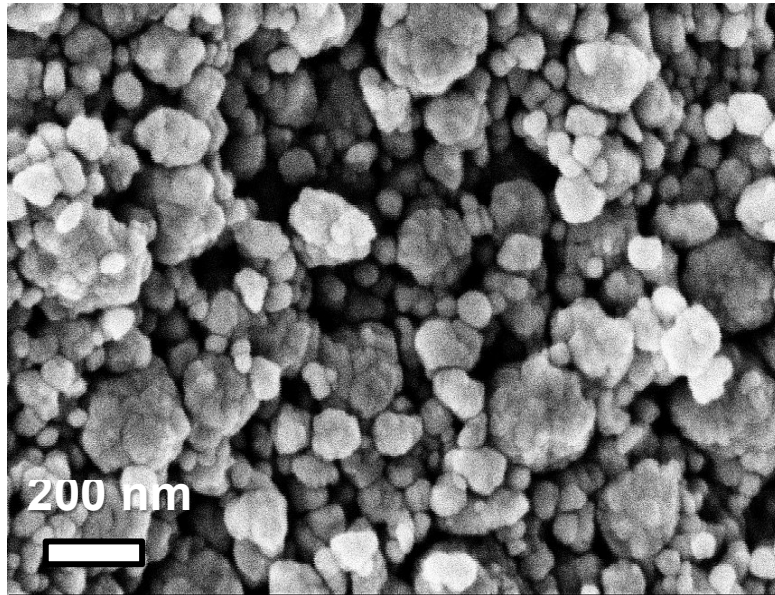


Figure 4: SEM image of Sample C

2.1.2 Experimental Setup and Sample Containment

The high-energy X-ray diffraction experiment was carried out at the 1-ID beamline at the Advanced Photon Source at Argonne National Laboratory. Diffraction measurements were performed with a monochromatic 80.675 keV X-ray beam with a beam size of $100 \times 100 \mu\text{m}^2$. The experiment took X-ray diffraction measurements using the “Hydra” detector array, which consists of four area detectors (GE angio type). The distance between the sample and the detector was ~ 2.102 m. Similar experimental setups can be found in the studies in refs. [1-5].

According to the APS radioactive experimental protocol, all radioactive samples need a double-layer containment to avoid possible leakage of radioactive materials. Fig. 5 shows Samples A-C loaded on the Ni-alloy sample stand for X-ray measurement. All these nano-grained UO_2 samples were contained in double-layer sample containers. An IR furnace able to provide up to 1300°C was slightly open to allow diffracted X-ray passing. Although there was no thermal annealing for the samples in this experiment, the same experimental setup will be applied to the future synchrotron scattering experiment with *in-situ* isothermal annealing.

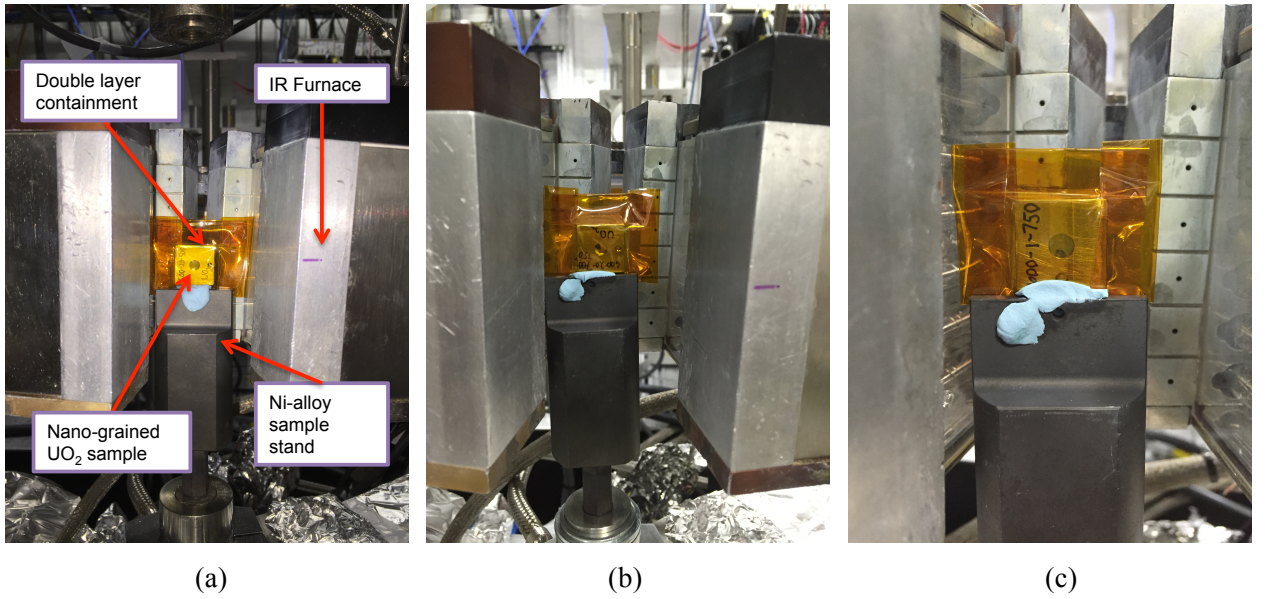


Figure 5: loaded nano-grained UO_2 samples on Ni-based stands: (a) Sample A; (b) Sample B; (c) Sample C.

2.2 Art of Synchrotron Scattering Data Analysis

The WAXS data from a polycrystalline specimen contains a set of information about its microstructural characteristics. The most fundamental information that can be obtained is the spacings of atomic layers, namely, the d-spacings. The d-spacings correspond directly to the positions of the diffraction peaks in the WAXS spectrum. According to Bragg's law,

$$2d_{hkl}\sin\theta_{hkl} = \lambda,$$

where λ is the wavelength of the monochromatic X-ray photons, θ is the diffraction angle, d is the d-spacing of a specific atomic layer, and the subscript $\{hkl\}$ is the Miller's index of that atomic layer. In cubic structure materials such as our material of interest, UO_2 , the d-spacing of a specific reflection $\{hkl\}$ can be related to the lattice constant, a_0 , through the following equation,

$$d_{hkl} = \frac{a_0}{\sqrt{h^2+k^2+l^2}},$$

Therefore, the lattice constant of the specimen can be straightforwardly measured according to the position of the diffraction peaks collected in WAXS investigations.

As the Hydra detector array is capable of collecting a full 360° azimuth angle of diffraction information, a 10° azimuth interval was selected to fit the diffraction peaks. The pseudo-Voigt peak function was assumed for the peak fitting. For each reflection, the measured d-spacing value was averaged as described by the following equation,

$$\overline{d_{hkl}} = \frac{\sum_j I_{hkl}^j d_{hkl}^j}{\sum_j I_{hkl}^j},$$

where the superscript j is the index of different azimuth interval, I_{hkl}^j is the integrated intensity of the $\{hkl\}$ reflection within that azimuth interval. The final lattice constant value was thereafter averaged over 10 reflections with the lowest Miller indices.

Aside from the lattice spacing information discussed above, the WAXS data also includes information about the internal strain and grain size. The interpretation of those properties, however, requires more complex processing of the broadening of diffraction peaks. One conventional approach that differentiates the grain size and internal strain the contributions to peak broadening is called the Williamson-Hall (W-H) analysis. The contributions to peak breadth due to grain size and internal strain have different dependencies on the diffraction angle. In the simplified W-H analysis, it is assumed that the overall broadening of a peak is a simple sum of the size and strain broadening contributions, and the relationship can be described as:

$$\beta \cos \theta = C \varepsilon \sin \theta + K \lambda / D,$$

where β is the breadth of a specific reflection peak, θ is the diffraction angle, ε is the internal strain, λ is the wavelength of the photon, D is the grain size, C and K are adjustable constants.

However, the internal strain ε can originate from different sources. Strains from various origins may influence the peak broadening through different mechanisms. That is, the linear assumption in the W-H analysis is likely to be unrealistic in some cases. For instance, when the internal strain is dominated by isotropically and uniformly distributed dislocations or dislocation loops, the W-H analysis is no longer the best interpretation of the peak broadening. Instead, Ungar et al. modified the W-H method so as to adapt it to the situation described above. In the modified W-H analysis, the dislocation density within the X-ray-illuminated volume can be measured [6]:

$$\Delta K = \frac{0.9}{D} + \left(\frac{\pi A^2 b^2}{2} \right)^{\frac{1}{2}} \rho^{\frac{1}{2}} (K \bar{C}^{\frac{1}{2}}),$$

where A is an adjustable parameter ranging from 1 to 2 for dislocation density between 10^{14} to 10^{15} m^{-2} levels, b is the length of the Burgers vector, ρ is the dislocation density, \bar{C} is the contrast factor, $K = 2 \sin \theta / \lambda$, and $\Delta K = 2 \cos \theta \Delta \theta / \lambda$. \bar{C} is determined by the crystal structure and stiffness tensor of the material. The stiffness tensor of UO_2 at different temperatures has been measured by inelastic neutron scattering [7].

The pseudo-Voigt function that was used for peak fitting has two components:

$$pV(2\theta) = I_0[\eta L(2\theta) + (1 - \eta)G(2\theta)],$$

where I_0 is the peak intensity, $L(2\theta)$ is the Lorentzian component, $G(2\theta)$ is the Gaussian component, and η is the weight of the Lorentzian component. The breadth of the peak then has the following form:

$$\beta = \Delta \theta = \omega [\pi \eta + (1 - \eta) \left(\frac{\pi}{\ln 2} \right)^{\frac{1}{2}}],$$

where ω is the half of the peak's FWHM. The instrumentation broadening that is measured by a powder ceria specimen must be eliminated from the measured peak broadening before completing this analysis. The values of \bar{C} for edge (\bar{C}_e) and screw (\bar{C}_s) dislocations are different. This difference can be utilized to quantify the fraction of the screw dislocations, ν_s , and, more importantly, improve the confidence of the modified W-H fitting. To do this, two parameters of \bar{C} need to be averaged separately as suggested by Ungar et al.[8]:

$$\bar{C} = \bar{C}_{h00}(1 - qH^2),$$

where \bar{C}_{h00} is the average contrast factor of $\{h00\}$ reflections, q is a material characteristic parameter, and $H^2 = (h^2k^2 + h^2l^2 + k^2l^2)/(h^2 + k^2 + l^2)^2$ is a reflection parameter. Assuming both edge and screw dislocations exist in the crystal, \bar{C} has the following expression:

$$\bar{C} = [\nu_s \bar{C}_{h00,s} + (1 - \nu_s) \bar{C}_{h00,e} \{1 - [\nu_s q_s + (1 - \nu_s) q_e] H^2\}],$$

The ν_s that maximizes the coefficient of determination (R^2) when fitting the modified W-H equation was regarded as the optimized fraction of screw dislocations in the specimen. The specific parameters that were used to calculate the contrast factors are listed in Table 2.

Table 2: the parameters used in the calculation of contrast factors.

Parameter	Values (r.t.)
c_{11}	389.3 GPa[7]
c_{12}	118.7 GPa[7]
c_{44}	59.7 GPa[7]
$A=2c_{44}/(c_{11}-c_{12})$	0.44124
$\overline{c_{12}/c_{44}}$	1.98827
$\overline{C}_{h00,s}$	0.1143
$\overline{C}_{h00,e}$	0.1298
q_s	-0.6798
q_e	-1.8121

2.3 Results and Discussion

2.3.1 Lattice Parameter Measurement

The WAXS data collected by 2D detectors were first azimuthally integrated to provide a relationship between intensity and diffraction angle, or d-spacing, as shown in Figure 6. The results are consistent with the previous data collected by conventional XRD. Only a single fluorite phase was identified except in sample A. In sample A, a series of weak peaks were found (note the logarithmic scale), which were not included in the previous XRD scanning of the same sample. These peaks are likely due to the oxidization (e.g. U_4O_9 and U_3O_7) of UO_2 during storage and shipment. As grain growth rather than oxidation is the focus of this study, the successive discussion will concentrate on the fluorite phase.

The lattice constants were first measured according to Bragg's law. Meanwhile, the stoichiometry of UO_{2+x} can also be deduced using the empirical linear relationship[9]:

$$a_0 = 5.4696 - 0.1495x.$$

The results are listed in Table 3.

Table 3: lattice constants and stoichiometry of the samples

Sample Index	A	B	C
Lattice constant, $a_0/\text{\AA}$	5.4266	5.4608	5.4642
Stoichiometry, x	0.2876	0.0843	0.0361

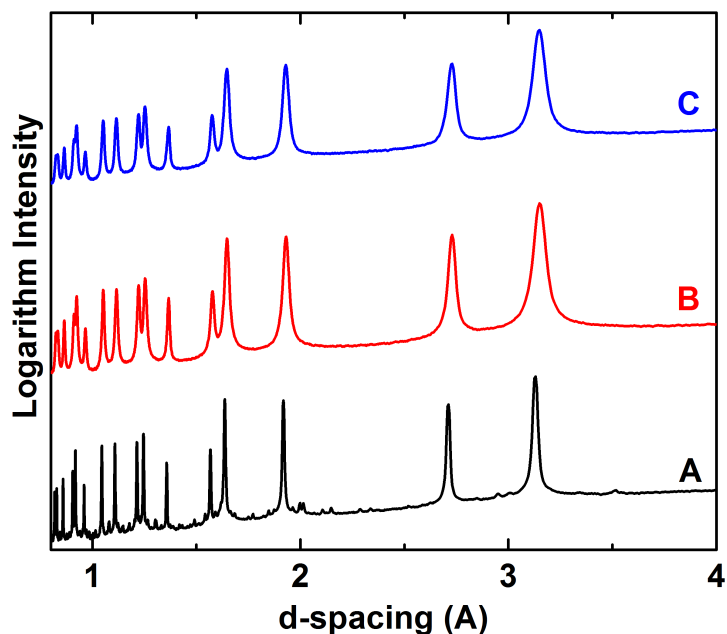


Figure 6: lineouts of WAXS scattering results

According to Table 3 and Figure 6, the 500 MPa sintered sample shows very different features compared with 750 MPa sintered ones, including higher stoichiometry and broader diffraction peaks. The latter implies smaller grains or denser dislocations, which will be discussed in the next section.

2.3.2 The Williamson-Hall Analysis

Both conventional and modified Williamson-Hall analyses were carried out for the three UO_2 samples so as to measure the grain size as well as the dislocation density.

The results of both W-H analyses for Sample A are illustrated in Figures 7 and 8. In this sample, the grain size was measured to be 140.6 nm. As previously mentioned, the grain size of the same sample was determined to be 99 nm according to SEM images. The difference could be interpreted as the combination of the surface effect and limited number of measured grains in SEM investigation. On the other hand, the dislocation density in Sample A is low.

The results of Sample B are shown in Figures 9 and 10. The grain size is approximately half of that in Sample A. This finding is also consistent with the SEM observation as shown in Figures 2 and 3. Also, this sample has a relatively high dislocation density, approximately two orders of magnitude higher than that in Sample A.

Shown in Figures 11 and 12 are the analyses for Sample C. Sample C has a grain size comparable to that of Sample A. Meanwhile, the dislocation density of Sample C is even higher than that of Sample B. A summary of the W-H analysis results are listed in Table 4.

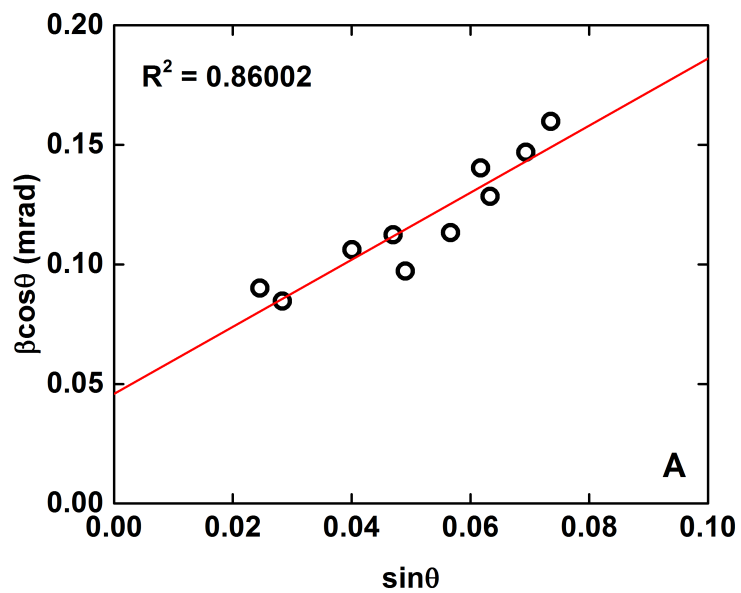


Figure 7: the conventional W-H analysis of Sample A

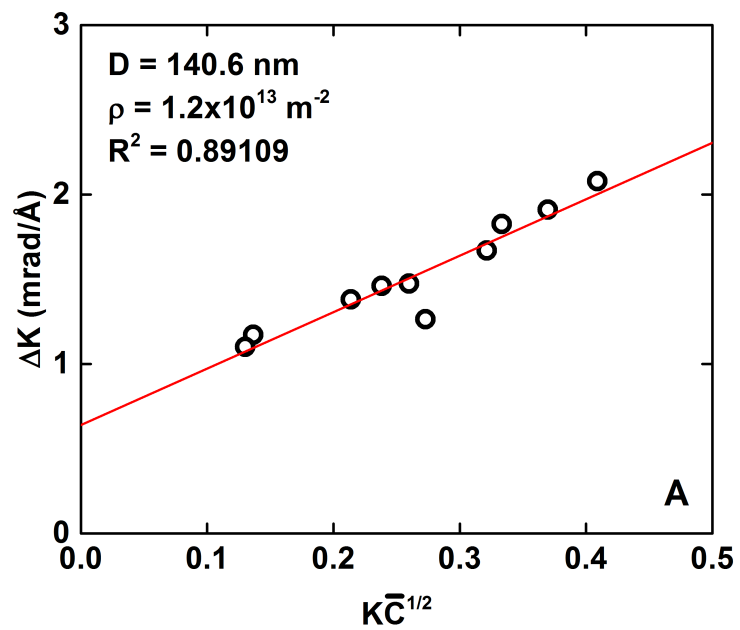


Figure 8: the modified W-H analysis of Sample B

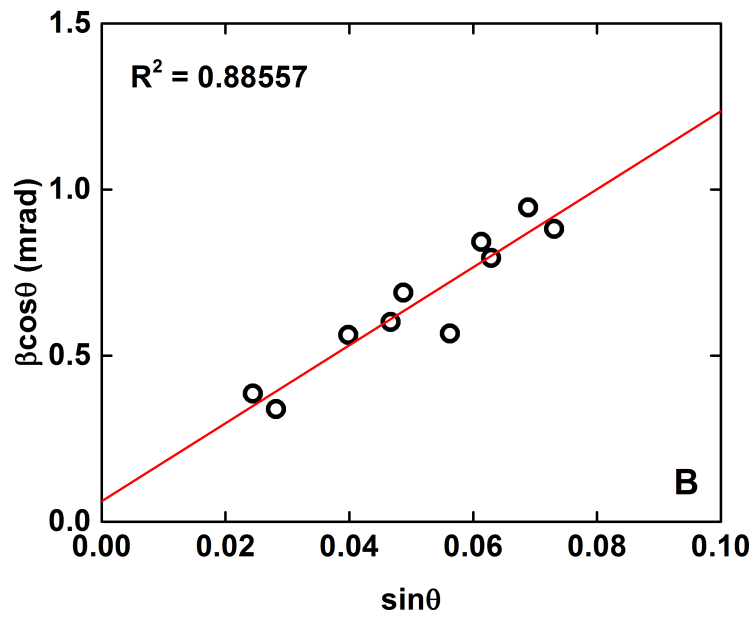


Figure 9: the conventional W-H analysis of Sample B

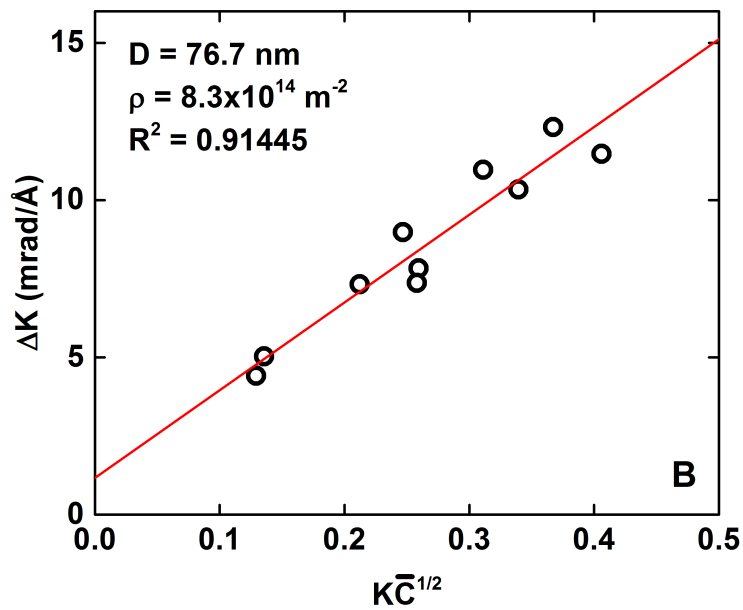


Figure 10: the modified W-H analysis of Sample B

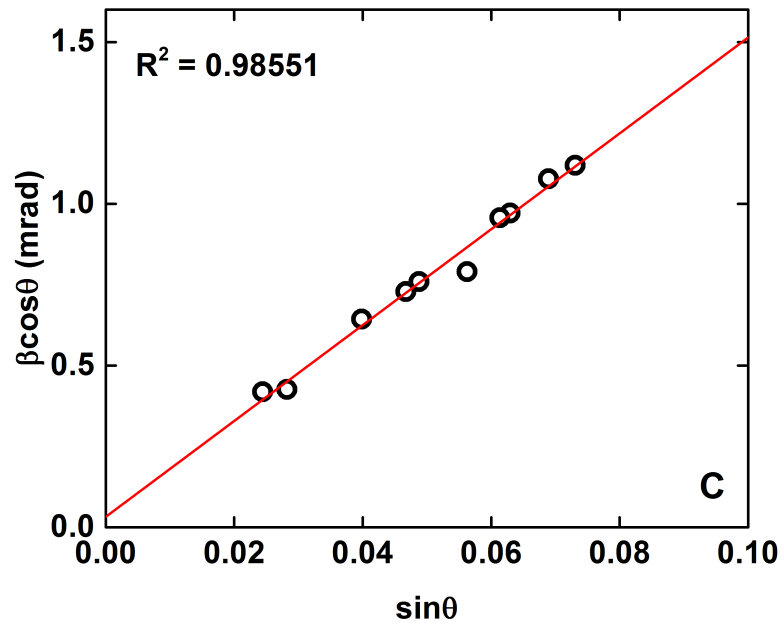


Figure 11: the conventional W-H analysis of Sample C

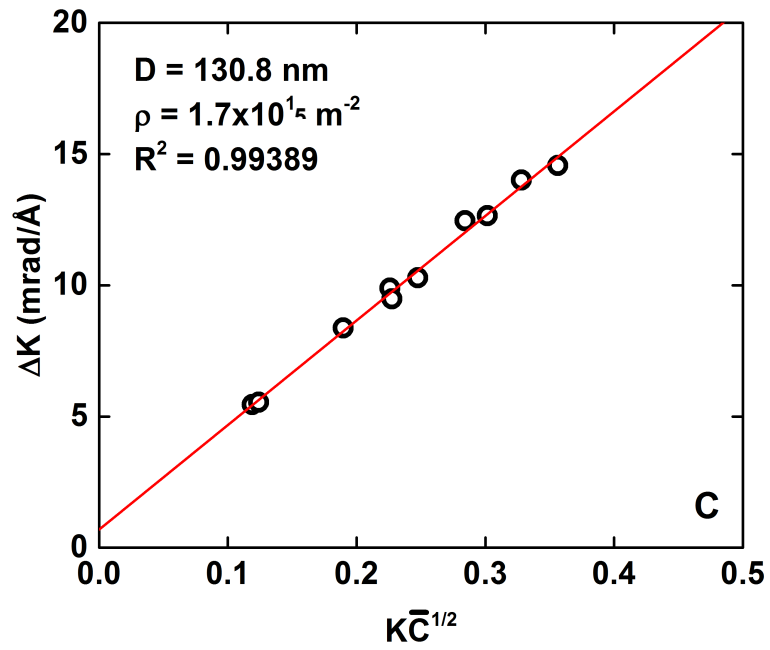


Figure 12: the modified W-H analysis of Sample C

Table 4: fitting results of the conventional and modified W-H analyses

			A	B	C
Conventional W-H	K/D	mrad/Å	0.298	0.402	0.216
	$C\varepsilon$	mrad	1.403	11.743	14.808
	R^2	n/a	0.86002	0.88557	0.98511
Modified W-H	D	nm	140.6	76.7	130.8
	ρ	$\times 10^{14} \text{ m}^{-2}$	0.12	8.30	1.69
	R^2	n/a	0.89109	0.91445	0.99389

For all three samples, the modified W-H analysis gives a better linearity compared to the conventional one, indicating that the interpretation of internal strain used in the modified W-H analysis is suitable for the UO_2 samples. Samples B and C, which were sintered at higher pressure, contain a higher density of dislocations, implying the effect of sintering pressure.

In this synchrotron study, both the grain size and dislocation density were measured by means of the synchrotron X-ray scattering technique. The success of this effort demonstrates the feasibility of employing this advanced method in our prospective in situ grain growth measurement. It is also worth mentioning that the monochromator used in this study provides a 10^{-4} resolution. An advanced monochromator with 10^{-5} resolution is also available at the same beamline for our future experiments, which is capable of improve the accuracy of our measurement by an order of magnitude.

3. Isothermal Annealing and Grain Growth Kinetics

Grain growth behavior of bulk micron sintered UO_2 fuel was widely studied at 1960~70s. Fuel properties degrade with burn-up degree. Specifically, at rim part of fuel where undergoes highest neutron density, after local burn up reaches to ~ 50 GWd/tHM, microstructure reconstruction initiates, mainly involving micron size pores over-pressured by fission gas and submicron size fresh grains from grain subdividing.

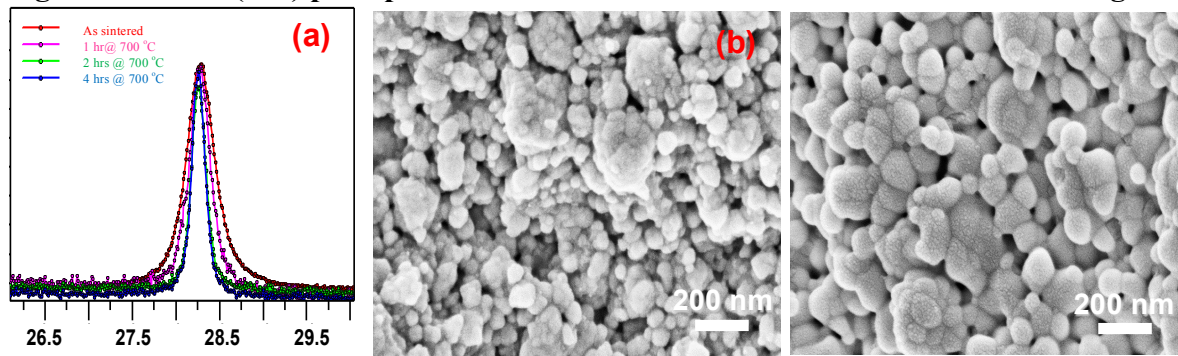
Due to experimental difficulties, the exact formation mechanism of such rim structure is still unclear, however, its effect on fuel performs is critical. Firstly, deeper fuel burn-up extends lifetime of fuel rods and thus cuts down the volumetric size of nuclear waste. However, this advance should not at the sacrifice of reactor safety margin if HBS has negative effect on fuel performance as burn up goes deeper. Secondary, development of NEAMs tool kit which focuses fuel preformation estimation based on microstructure requires a thorough understanding of the rim structure before its behavior can be modeled.

In this study, dense ($> 95\%$ TD) nano and submicron UO_2 pellet with various stoichiometry were thermal annealed under argon atmosphere to explore its stability over roughly the actual temperature for HBS (600-800 $^\circ\text{C}$). Grain growth behavior was analyzed based on the effect of porosity and stoichiometry on grain boundary migration. Derived kinetic values, including activation energy and time component was compared with literature ones. Various mass transport mechanisms are compared and grain boundary mitigated diffusion is suggested to be responsible for UO_2 at the studied grain size level. Data provided in this study would serve as preliminary starting point for HBS modeling.

3.1 Isothermal Annealing and Grain Growth Characterization

Thermal annealing of sample was done by MTI @ GSL-1100X-UL tube furnace in ultra-pure Argon gas flow at 7 $^\circ\text{C}$ to 900 $^\circ\text{C}$ from 0.5 hr to 8 hrs. Samples for SEM grain size characterization were collected by fracturing the bulk sample so as to reveal both grain boundary and pore distribution. For each data for grain size of UO_2 , at least 200 grains are counted. A mean value of the grain size is derived, and the uncertainty of the grain size is evaluated based on the standard deviation of the mean.

Figure 13: XRD (111) peak position and width for 7-1- $\text{UO}_{2.03}$ after various holding time at



700 $^\circ\text{C}$ (a), microstructure of 7-1- $\text{UO}_{2.03}$ after 2 hrs (b) and 4 hrs (c) holding at 700 $^\circ\text{C}$ (Yao and Lian, unpublished data).

Before isothermal annealing, the effects of the annealing atmosphere on the stoichiometry and structural integrity of the sintered fuel pellets were investigated first, and the oxidation of the sintered fuel pellets was obtained. Oxidation of the pure stoichiometric nano-sized UO_2 pellets to hyperstoichiometry composites or secondary phase formation of U_3O_8 were observed, leading to the pulverization of sintered pellets above temperature 600 $^\circ\text{C}$. The oxidation of the sintered nano- UO_2 was also identified after storage of the sintered pellets in an ambient condition. These results suggest the

importance of the confinement of the storage of the sintered fuel pellets in order to mitigate the oxidation issues and resulting chemical composition variation as a result of strong oxidation potential of the uranium. Therefore, all of the isothermal annealing was performed on a protective environment within Ar to avoid the oxidation. Figure 13 shows XRD diffraction and the SEM images of the nano-sized $\text{UO}_{2.03}$ with initial grain size of ~ 40 nm upon annealing at 700°C for 4 hrs. A significant grain coarsening occurred with the average size of 94 ± 15 nm. No oxidation was observed as evidenced by the consistent XRD diffraction spectrum without peak shifting, suggesting that the grain growth kinetics can be well attained by isothermal annealing under protective environments.

3.2 Grain Growth Kinetics

The grain growth kinetics was investigated by isothermal annealing combining with *ex-situ* SEM observation on microstructure evolution and grain size determination. Nano-sized $\text{UO}_{2.03}$ and $\text{UO}_{2.11}$ fuel pellets with different initial grain sizes were chose as the target materials, and the annealing was performed at controlled argon environments at different temperatures ($600 \sim 900^\circ\text{C}$ and $0.5 \sim 8$ hrs). Microstructure analysis of the annealed fuel pellets and measurement of the grain size were performed as functions of annealing temperature, duration and stoichiometry. The current experimental data on the grain growth are being analyzed, and the grain growth exponent and activation energy, and the effects of stoichiometry on UO_2 grain growth kinetics are analyzed and compared with MD simulations and experimental data on large-sized UO_2 in literatures.

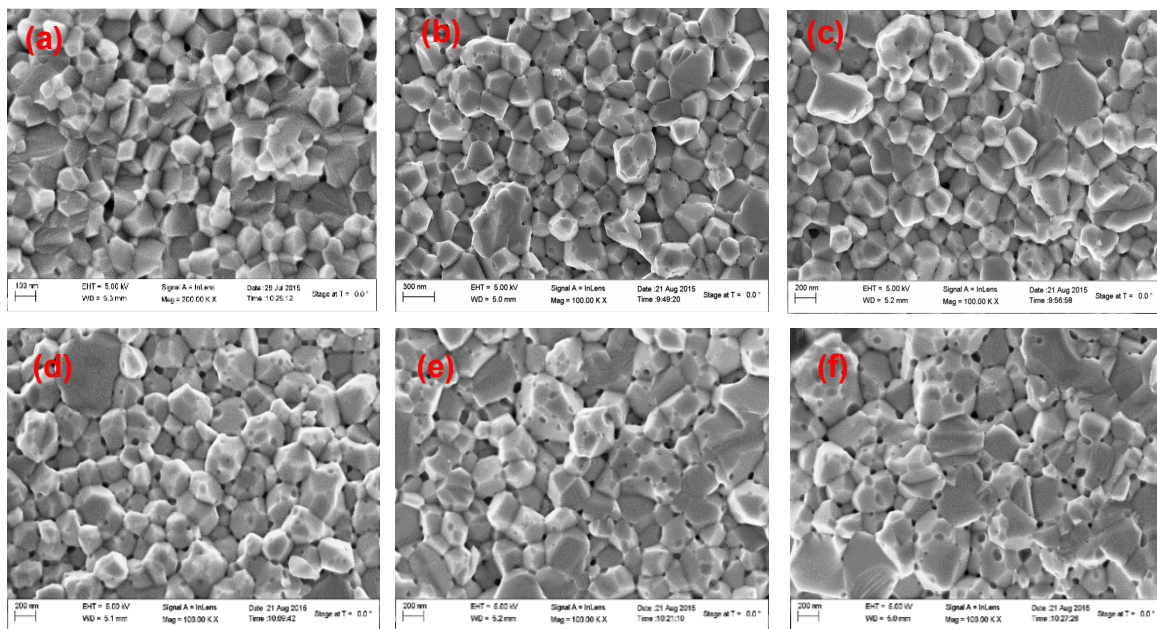


Figure 14: microstructure of 7-5- $\text{UO}_{2.03}$ after 0 hr (a), 0.5 hr (b), 1 hr (c), 2 hrs (d), 4 hrs (e), and 8 hrs (f) holding at 700°C (scale bar is 200 nm except for 100 nm in (a) and 300 nm in (b)) (Yao and Lian, unpublished data).

Fig. 14 shows SEM images of the 7-5- $\text{UO}_{2.03}$ after various duration of holding at 700°C . Grain grows from the starting size of 103 nm to 155 nm, 166 nm, 189 nm, 239 nm, and 138 nm after 0.5 hr, 1 hr, 2 hrs, 4 hrs, and 8 hrs annealing, respectively. A slight increase in the pore size was observed accompanying with grain coarsening, and majority of the pores are identified to be distributed at grain boundaries. A further increase in the grain size was also observed for the samples annealed at higher temperatures of 800°C and 900°C . The grain size increases to 341 nm after 8 hrs annealing at 800°C . Pores also grow with grains and majority of them locates on grain boundary triple junction area.

For the sample of the 7-20-UO_{2.03} within initial grain size of 144 nm, grain size increases to 167 nm, 194 nm, 202 nm, 197 nm, and 185 nm after 0.5 hr, 1 hr, 2 hrs, 4 hrs, and 8 hrs annealing, respectively. The averaged grain size after 8 hrs annealing is smaller than the 4 hrs annealing samples, indicating abnormal grain growth is involved. Grain size further increases to 273 and 377 nm after 8 hrs annealing at 800 and 900 °C, respectively.

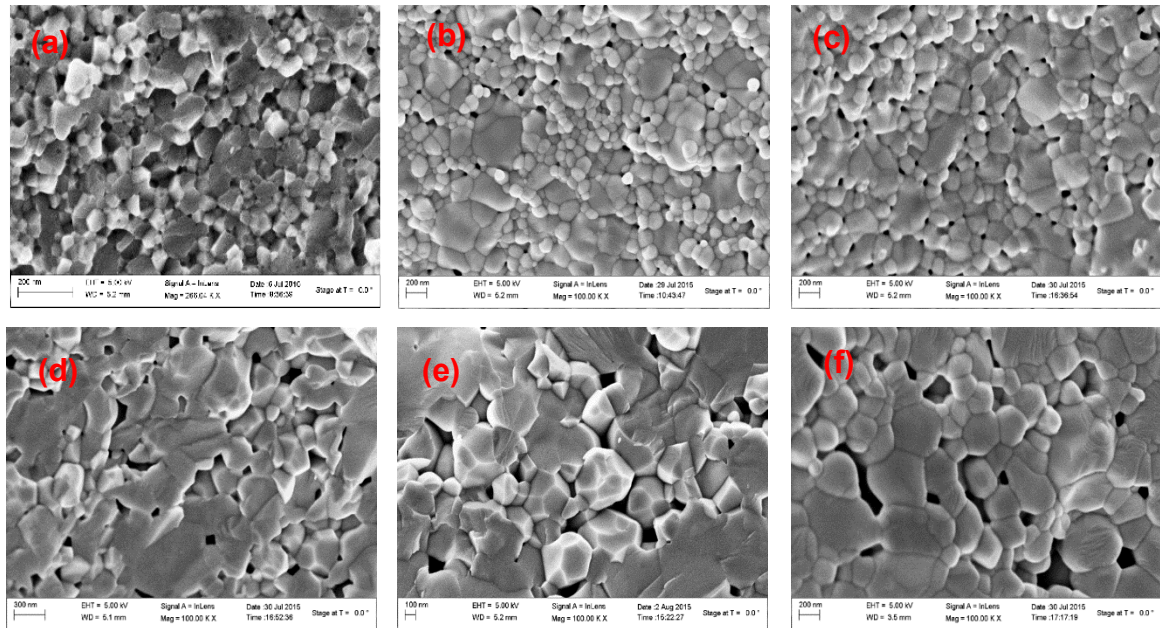


Figure 15: microstructure of 6-20-UO_{2.11} after 0 hr (a), 0.5 hr (b), 1 hr (c), 2 hrs (d), 4 hrs (e), and 8 hrs (f) holding at 700 °C (scale bars are 200 nm except for 300 nm in (d) and 100 nm in (e)) (Yao and Lian, unpublished data).

Fig. 15 shows the 6-20-UO_{2.11} after various duration of holding at 700 °C. Grain grows from the starting size of 63 nm to 295 nm, 338 nm, 452 nm, 464 nm, and 499 nm after 0.5 hr, 1 hr, 2 hrs, 4 hrs, and 8 hrs annealing, respectively. Grain growth is much more appreciable than UO_{2.03} samples. A distinct feature can be observed in which pores also grow to much bigger size and interconnected with each other upon isothermal annealing. Grain grows to 770 nm and 2160 nm after 8 hrs annealing at 800 and 900 °C, respectively.

Fig. 16 summarizes the correlation among the grain coarsening for stoichiometric UO₂ and UO_{2.11} with different initial grain sizes as function of duration and annealing temperature. Major finds include followings:

- (1) Grain size increases exponentially with time in relatively short duration of 0-2 hrs upon isothermal annealing. Higher annealing temperature leads to large grain size increases as a result of enhanced grain boundary mobility.
- (2) With further increase of annealing time, grain size increase saturates due to the loss of drive force resulting from curvature driven-growth process.
- (3) Initial grain size has a minimal effect on the grain coarsening kinetics, and no significant variation in the grain growth was observed for sintered UO₂ fuel pellets.

(4) Pore size of the sintered fuel pellets increases for both stoichiometry and hyper-stoichiometric compositions but with drastically morphological variation. Closed inter-granular pores are observed in nano-sized UO_2 ; in contrast, in $\text{UO}_{2.11}$, interconnected pores form upon isothermal annealing, which may significantly affect the coarsening kinetics by pinning the grain boundary migration.

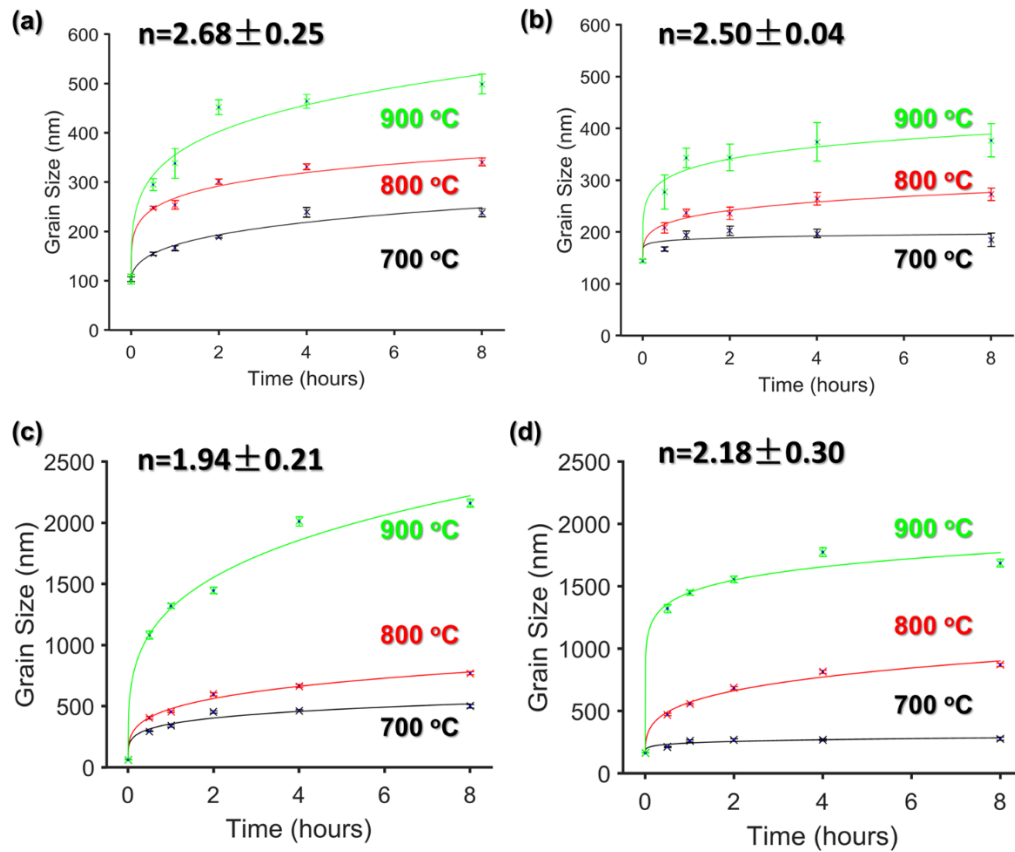


Figure 16: grain growth data curve fitting with fitted growth component highlighted for 7-5- $\text{UO}_{2.03}$ (a), 7-20- $\text{UO}_{2.03}$ (b), 6-20- $\text{UO}_{2.11}$ (c), and 7-20- $\text{UO}_{2.11}$ (d) (Yao and Lian, unpublished data)

(5) Stoichiometry of the sintered UO_2 fuels significantly impacts the grain coarsening processing, in which hyper-stoichiometric compositions with oxygen enrichment display greater tendency toward grain coarsening, leading to the larger grain size. For example, the effect of stoichiometry on grain growth behavior of dense nano UO_2 can be appreciated by comparing experimental results on 7-20- $\text{UO}_{2.03}$ and 7-20- $\text{UO}_{2.11}$ sample. Both of them have similar density and grain size, except for the stoichiometry. Under all annealing conditions, the 7-20- $\text{UO}_{2.11}$ sample always shows larger grain size. Larger grain size in the 7-20- $\text{UO}_{2.11}$ samples reduces pore number and explains its bigger pores than 7-20- $\text{UO}_{2.03}$ samples.

The enhanced grain coarsening kinetics is consistent with the greater sinterability of the oxygen-enriched composite for densification. Excessive oxygen in UO_{2+x} occupies interstitial position, leading to vacancies in U sublattice based on Frenkel pair defect model and thus enhancing the U ion diffusion rate. UO_{2+x} powders with a slight hyper-stoichiometry are regularly used as the starting materials for fuel fabrication. There is no density measurement conducted in the annealed sample, and thus we cannot confirm grain growth induced densification found in bulk micron UO_2 samples. However, we do found substantial amount of pores locates on grain boundary grows with grain size, showing grain growth is much more rapid than pore elimination.

3.3 Grain Coarsening Kinetics

Grain growth data curves are fitted by Mat lab with 95% confidence bounds based on the following equation

$$D^n - D_0^n = k_0 e^{\left(\frac{-Q}{RT}\right)} t^m \quad (1)$$

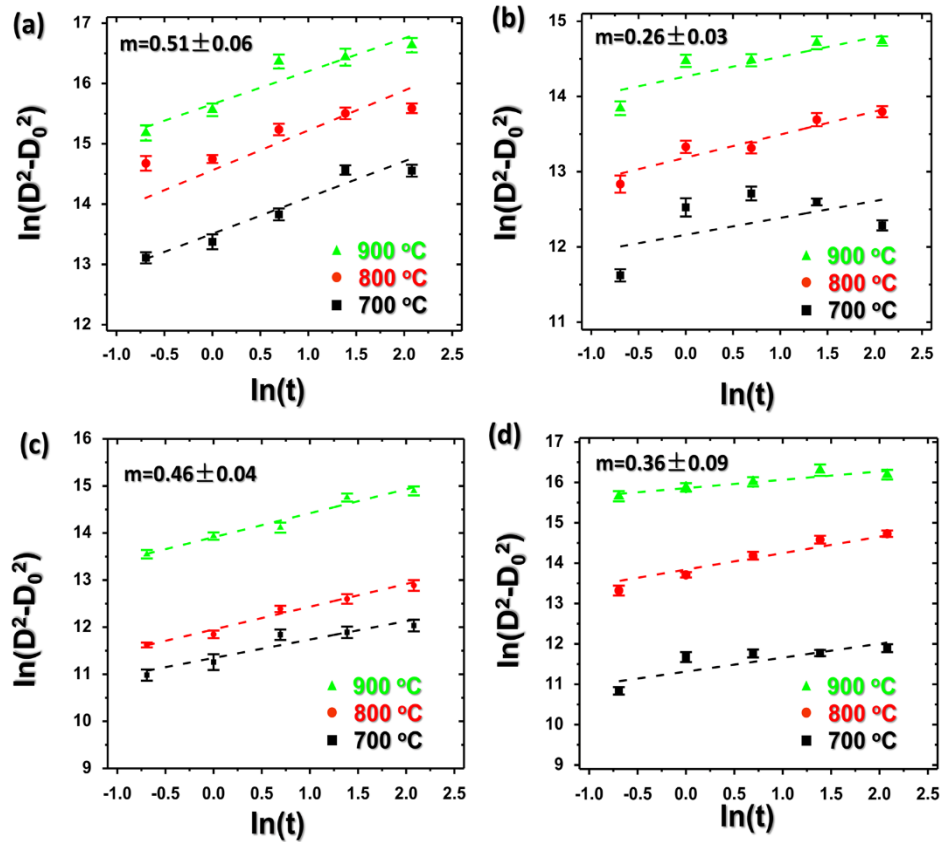
Where D is grain size of sintered urania sample after annealing at certain temperature for a given span of time; D0 is the starting grain size in the sintered urania sample; n is grain growth component; K0 is fitting constants; Q is grain growth activation energy; R is gas constant; T is temperature in K, and t is annealing time in hr; m is time component.

Doing natural log on both sides of equation (1) leads to following equation:

$$\ln(D^2 - D_0^2) = \ln K_0 - \frac{Q}{R} \times \frac{1}{T} + m \ln t \quad (2)$$

As a result, plot $\ln(D^2 - D_0^2)$ with respect to $\frac{1}{T}$ provides values of $-\frac{Q}{R}$ as the slope of plotting and further Q, Similarly, plot $\ln(D^2 - D_0^2)$ with respect to $\ln t$ delivers values of m.

Figure 17: grain growth time component fitting for 7-5-UO_{2.03} (a), 7-20-UO_{2.03} (b), 6-20-



UO_{2.11} (c), and 7-20-UO_{2.11} (d) (Yao and Lian, unpublished data).

The grain growth components can be derived from the fitting of the experimental grain coarsening data (as shown in Fig. 16). With experimental uncertainty, the grain growth components are within the range of 2-3, suggesting a standard thermal driven growth process as driven by the grain curvature with the grain component of 2. Grain growth component of 3 was found most appropriately describing pore influenced grain growth of bulk micron UO₂. For those bulk samples, the remaining pores have sizes bigger than 1 micron, and vapor condensation is proposed as the controlling mechanism for grain

boundary migration [10]. The relative importance of this transport mechanism with others, such as surface diffusion and volume diffusion, was discussed in Ref. [11] based on effect of pore size. Surface diffusion dominates small pores; while volume diffusion at intermediate size, and vapor condensation when pore size is large enough. Size of the remaining pores in our sintered pellet is at tens nano size scale before thermal annealing and stays smaller than 1 μm after. Therefore, surface or grain boundary diffusion may dominate the mass transport mechanisms for the grain growth and pore coalescence processes.

Both time component (Fig. 17) and activation energy (Q) (Fig. 18) can also be derived, show overall good linear fitting features. The activation energy of the stoichiometric UO_2 is less than 1 eV for both samples with different initial grain sizes, significantly lower than the previous reported values from micron-sized UO_2 fuel matrix and MD simulations in which a bi-crystal model is assumed. Grain boundaries are considered as 2D plane with high concentration of point defect. Those defects have dramatically influence over mass transportation near grain boundaries. Experimental study shows uranium self-diffusion coefficient near grain boundary is five orders magnitude higher than it in single-crystal. Simulation study also shows the migration energies for U ions near grain boundary is as low as 0.8 eV [12], compared with simulated value of 4.4 eV for vacancy migration and 5.8 eV for interstitial migration.

In our study, thermal annealing is carried out between 700-900 $^{\circ}\text{C}$, much lower than previously studied temperature range roughly at 1500-2000 $^{\circ}\text{C}$ for grain coarsening study in bulk UO_2 . At low temperature, grain boundaries mitigated U ion migration plays a much more important role than other mechanism as the latter ones are strongly depends on prevalence of point vacancies which proportionally depends on temperature. Q values derived for the four samples are higher than the aforementioned migration energy for U ions at grain boundary, but lower than vacancy and interstitial migration ones, indicating the grain growth behavior is affected by mixed mass migration mechanism. Therefore, the activation energy for grain growth is similar to the energy barrier for grain boundary in nanocrystalline UO_2 , again suggesting the dominate mechanism of surface and grain boundary diffusion.

U ion diffusion is recognized as the rate-limiting step diffusion controlled process, including grain growth. To facilitate UO_2 powder densification, a slightly oxidized atmosphere is utilized to introduce extra oxygen into the UO_2 lattice to enhance U ion diffusion so as to promote pore elimination and grain growth. Therefore, hyperstoichiometric UO_{2+x} are generally considered to have lower activation energy for grain growth and this hypothesize is validated through experiment and simulation study. Results presented here shows the $\text{UO}_{2.11}$ samples have higher activation energy of ~ 2 eV, significantly greater than that of $\text{UO}_{2.03}$ samples. This is contradicted to previously understanding on the effect of stoichiometry on grain growth of UO_2 . The greater activation energy for hyper-stoichiometric composition may be associated with the pore structures in which an interconnected pore structure forms to pin the grain boundary migration, and vapor condensation may dominate the mass transport mechanism.

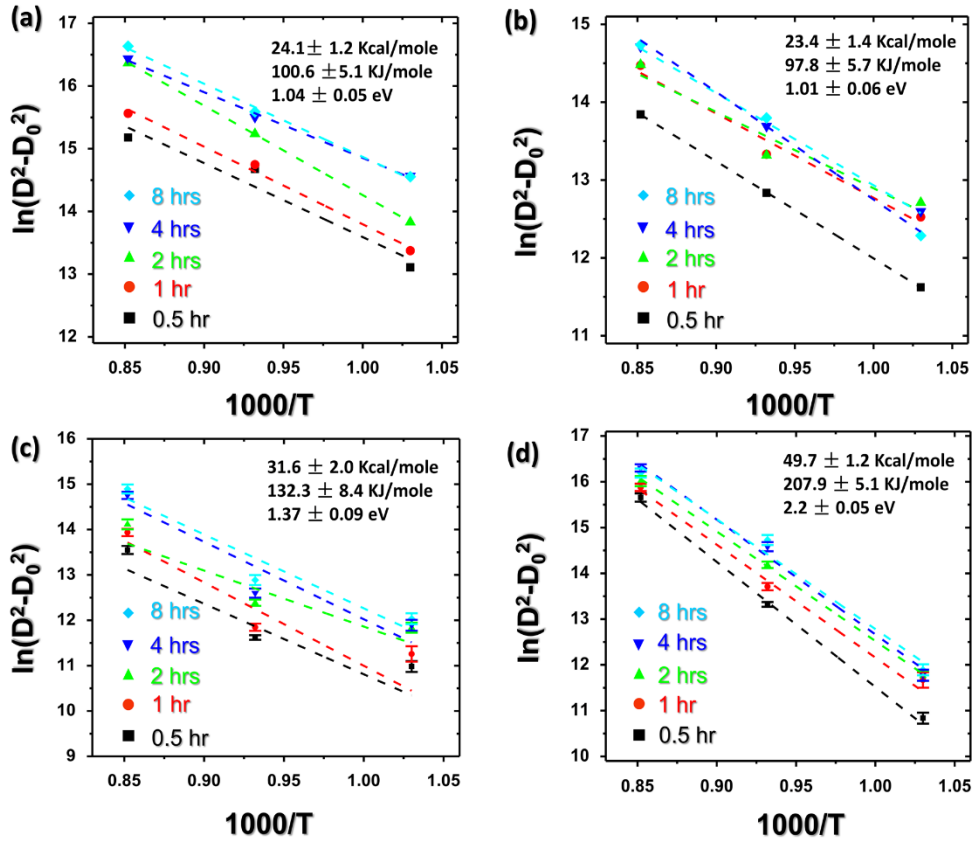


Figure 18: grain growth activation energy fitting for 7-5- $\text{UO}_{2.03}$ (a), 7-20- $\text{UO}_{2.03}$ (b), 6-20- $\text{UO}_{2.11}$ (c), and 7-20- $\text{UO}_{2.11}$ (d) (Yao and Lian, unpublished data).

Specifically, pores can pose a drag force similar to insoluble impurity of metal when grain boundary movement is activated. Suppose those pores attach to and move with grain boundary, the magnitude of the force is found by previous research on bulk micron UO_2 to be dependent on pore sizes. Basically, when pore size is larger than $0.1 \mu\text{m}$, pores tend to attach to grain boundaries and moves with them, and thus pose little effect over grain growth. On the other side, if the pore size is large than $0.1 \mu\text{m}$, it pins the grain boundary and are very effective in stopping boundary sweeping. In this study, limited porosity was evidenced by the high density and dense microstructure. However, the growth and migration of pores shows different features based on various level of porosity regardless of UO_2 stoichiometry. For example, pores in 7-5- $\text{UO}_{2.03}$ samples grows 2-3 times larger than the counterpart in 7-20- $\text{UO}_{2.03}$ samples after annealed at 900°C for 8 hrs. Also, the former have higher rate of lenticular shape and sits between two grain boundaries, some of the bigger pores interconnect with each other. Instead, the latter mostly locates on the triple junction area with equilateral triangle shapes and majority of those pores isolate from each other.

4. Future Work

In FY15, we have completed a methodology study using synchrotron X-rays to analyze the grain growth of nano-grained UO_2 . We also completed a systematic grain growth analysis of nano-sized $\text{UO}_{2.03}$ and $\text{UO}_{2.11}$.

To completely understand the grain growth kinetics of nano-grained UO_2 , *in-situ* characterization of the entire stage of grain growth from the very beginning of the isothermal annealing will be needed. *In-situ* characterization is particularly important for the early stage of grain growth which is difficult to record in *ex-situ* measurements. All experimental setup and data analysis procedures developed in this fiscal year can apply to the diffraction data taken from the future *in-situ* measurements. The only outstanding issue is meeting the stringent requirement for containing radioactive materials at APS. The old sample holder design was required to include one more layer of containment for the UO_2 samples. The new sample holder design was completed, and is under review by the safety committee at APS. The proposed *in-situ* grain growth experiment has been scheduled in the 2015-3 APS beam cycle. In addition to the grain growth experiments, we plan to perform nano-indentation/micro-hardness measurement of UO_2 materials with various grain sizes. This work aims at providing validation data for MARMOT and BISON Fracture Model.

The planned activities related to the nano-grained growth are listed below:

1. We will conduct a set of synchrotron experiments on UO_2 isothermally heated at a temperature in range of 700-1000°C (note: the temperature range was estimated from *ex-situ* SEM measurements done in FY15) to measure the grain growth. Complementary to the synchrotron measurements, transmission electron microscopy (TEM)/scanning electron microscopy (SEM) will be performed to provide direct images to support and validate the measured data obtained by synchrotron scattering. Based on the available materials at the time of the experiments, the impact of porosity and stoichiometry (UO_{2+x}) will be investigated.
2. We will begin working on the validation of the MARMOT and BISON Fracture Model. We will employ nano-indentation or small-scale micro-hardness measurement to determine the fracture toughness of UO_2 samples. The grain-size-dependent fracture toughness will be measured. Based on the available materials at the time of the experiments, the impact of grain boundaries on fracture toughness will also be studied.

5. Summary

This activity is supported by the US Nuclear Energy Advanced Modeling and Simulation (NEAMS) Fuels Product Line (FPL) and aims at providing experimental data for validation of the mesoscale simulation code MARMOT. MARMOT is a mesoscale multiphysics code that predicts the coevolution of microstructure and properties within reactor fuel during its lifetime in the reactor. It is an important component of the Moose-Bison-Marmot (MBM) code suite developed by Idaho National Laboratory (INL) to enable next generation fuel performance modeling capability as part of the NEAMS Program FPL. In order to ensure the accuracy of the microstructure-based materials models being developed within the MARMOT code, extensive validation efforts must be carried out. In this report, we summarize our work on methodology study of the use of synchrotron X-rays to measure the grain size of nano-grained UO_2 . In addition, investigation of grain growth kinetics was conducted based on isothermal annealing and grain growth characterization as functions of duration and temperature. The kinetic parameters, e.g., activation energy for grain growth for UO_2 , were obtained and compared for different stoichiometry and with molecular dynamics (MD) simulation results.

In addition to synchrotron radiation experiments, we completed several important methodology studies that are essential to the success of the planned *in-situ* measurements in FY16. The experimental setup for the high-temperature annealing experiment was configured at sector 1-ID. Three nano-grained UO_2 samples, sintered in different conditions, were exposed to high-energy synchrotron X-rays. The stoichiometry of each sample was determined from the measured lattice constants. The dislocation density and grain size of the nano-grained UO_2 samples were determined using both conventional and modified Williamson-Hall methods. In addition, the preliminary grain growth investigation of nano-grained UO_2 shows significant difference in grain coarsening kinetics between nanocrystalline and large-crystal UO_2 . Stoichiometry and porosity of the sintered UO_2 fuels were also found to significantly impact the grain coarsening process.

Further grain growth measurements of nano-grained UO_2 specimens have been planned. The synchrotron radiation experiment, assisted by TEM and SEM measurements, will be conducted in FY16. We also plan to further investigate the impact of stoichiometry and porosity on the grain growth kinetics of nano-grained UO_2 . Following the grain growth study, the fracture toughness of UO_2 with different grain sizes will be studied using nano-indentation or micro-hardness testing. All these measurement aim to provide validation data for physics models in MARMOT, including the grain growth model, the potential high-burnup-structure models (formation and stability), the porosity dragging model for grain growth, and the fracture model.

6. Acknowledgements

This work was supported under US Department of Energy Contract DE-AC02-06CH11357. We would like to thank the MARMOT development lead, Micheal Tonks, and MARMOT team member, Yongfeng Zhang, for providing very helpful guidance for this work.

7. References

1. Y. Miao, K. Mo, Z. Zhou, X. Liu, K. Lan, G. Zhang, M. K. Miller, K. A. Powers, J. Almer, J. F. Stubbins, "In-situ Synchrotron Tensile Investigations on the Phase Responses within an Oxide Dispersion-strengthened (ODS) 304 Steel," *Materials Science and Engineering: A*, Vol. 625, 146-152, 2015
2. K. Mo, Z. Zhou, Y. Miao, D. Yun, H. Tung, G. Zhang, W. Chen, J. Almer, and J. F. Stubbins, "Synchrotron study on load partitioning between ferrite/martensite and nanoparticles of a 9Cr ODS steel," *Journal of Nuclear Materials*, Vol. 455, 376–381, 2014
3. K. Mo, H. Tung, J. Almer, M. Li, X. Chen, W. Chen, J. B. Hansen, J. F. Stubbins, "Synchrotron radiation study on Alloy 617 and Alloy 230 for VHTR application," *Journal of Pressure Vessel Technology*, Vol. 135, paper No. 021502, 2013
4. G. Zhang, Z. Zhou, K. Mo, Y. Miao, X. Liu, J. Almer, J. F. Stubbins, "The evolution of internal stress and dislocation during tensile deformation in a 9Cr Ferritic/Martensitic (F/M) ODS steel investigated by high-energy X-rays," *Journal of Nuclear Materials*, Vol. 467, 50-57, 2015
5. Y. Miao, K. Mo, Z. Zhou, X. Liu, K. Lan, G. Zhang, M. K. Miller, K. A. Powers, Z. Mei, J. Park, J. Almer, J. F. Stubbins, "On the Microstructure and Strengthening Mechanism in ODS 316 Steel: A Coordinated Electron Microscopy, Atom Probe Tomography and In-situ Synchrotron Tensile Investigation," *Materials Science and Engineering: A*, Vol. 639, 585-596, 2015
6. T. Ungar, "Strain broadening caused by dislocations," *Materials Science Forum*, Vol. 278, 151–157, 1998
7. M. Hutchings, "High-temperature studies of UO_2 and ThO_2 using neutron scattering techniques," *J. Chem. Soc., Faraday Trans. 2*, Vol. 83, 1083-1103, 1987
8. T. Ungar, I. Dragomir, A. Revesz, A. Borbely, "The contrast factors of dislocations in cubic crystals: the dislocation model of strain anisotropy in practice," *Journal of Applied Crystallography*. Vol. 32, 992–1002, 1999
9. V.A. Alekseyev, L.A. Ananyeva, R.P. Rafalskiy, "Effects of composition on lattice parameter of UO_{2+x} ," *International Geology Review*, Vol. 23, 1229-1236, 1981
10. F. Nichols, "Theory of grain growth in porous compacts" *Journal of Applied Physics*, Vol. 37, 4599-4602, 1966
11. P. Shewmon, *Trans. Metall. Soc. AIME*, Vol. 230, 1134, 1964
12. E. Vincent-Aublant, J-M. Delaye, L. Van Brutzel, "Self-diffusion near symmetrical tilt grain boundaries in UO_2 matrix: A molecular dynamics simulation study," *Journal of Nuclear Materials*, Vol. 392, 114, 2009



Nuclear Engineering Division

Argonne National Laboratory
9700 South Cass Avenue, Bldg. 208
Argonne, IL 60439

www.anl.gov



Argonne National Laboratory is a U.S. Department of Energy
laboratory managed by UChicago Argonne, LLC